On the Supra-LUMO Interaction: Case Study of a Sudden Change of Electronic Structure as a Functional Emergence

Alexis Gosset, Štěpánka Nováková Lachmanová, Sawsen Cherraben, Gildas Bertho, Jérémy Forté, Christian Perruchot, Henri-pierre Jacquot Rouville, Lubomír Pospíšil, Magdaléna Hromadová, Éric Brémond, et al.

On the Supra-LUMO Interaction: Case Study of a Sudden Change of Electronic Structure as a Functional Emergence

Alexis Gosset,[a] Štěpánka Nováková Lachmanová,[b] Sawsen Cherraben,[a] Gildas Bertho,[c] Jérémy Forté,[d] Christian Perruchot,[a] Henri-Pierre Jacquot de Rouville,[a],[e] Lubomír Pospíšil,[b] Magdaléna Hromadová,*[b] Éric Brémond,*[a] Philippe P. Lainé*[a]

[a] A. Gosset, Dr. S. Cherraben, Dr. C. Perruchot, Dr. H.-P. Jacquot de Rouville, Dr. É. Brémond, Dr. P. P. Lainé
Université de Paris, CNRS, ITODYS, F-75006 Paris, France
E-mail: eric.bremond@u-paris.fr
philippe.laine@u-paris.fr

[b] Dr. Š. Nováková Lachmanová, Dr. L. Pospíšil, Dr. M. Hromadová
J. Heyrovský Institute of Physical Chemistry of the Czech Academy of Sciences, Dolejškova 3, 182 23 Prague, Czech Republic
E-mail: magdalena.hromadova@jh-inst.cas.cz

[c] Dr. G. Bertho
Université de Paris, Laboratoire de Chimie et Biochimie Pharmacologiques et Toxicologiques, CNRS UMR 8601, 45 rue des Saints-Pères, 75270 Paris Cedex 06, France.

[d] J. Forté
Sorbonne Université, UMR CNRS 8232, Institut Parisien de Chimie Moléculaire, 4 place Jussieu, 75005 Paris, France

[e] Dr. H.-P. Jacquot de Rouville
Present address: Université de Strasbourg, Institut de Chimie de Strasbourg (UMR CNRS 7177), Institut Le Bel, 4, rue Blaise Pascal, 67000 Strasbourg, France

Supporting information for this article is given via a link at the end of the document

Abstract

The synergistic functioning of redox-active components that emerges from prototypical 2,2'-di(*N*-methylpyrid-4-ylium)-1,1'-biphenyl is described. Interestingly, even if a *trans* conformation of the native assembly is expected, due to electrostatic repulsion between cationic pyridinium units, we demonstrate that *cis* conformation is equally energy-stabilized on account of a peculiar LUMO (SupLUMO) that develops through space, encompassing the two pyridiniums in a single, made-in-one-piece, electronic entity (superelectrophoric behavior). This SupLUMO emergence, with the *cis* species as superelectrophore embodiment, originates in a sudden change of electronic structure. This finding is substantiated by insights from solid state (single-crystal X-ray diffraction) and solution (NOE-NMR and UV-vis-NIR spectroelectrochemistry) studies, combined with electronic structure computations. Electrochemistry shows that electron transfers are so strongly correlated that two-electron reduction manifests itself as a single-step process with a large potential inversion consistent with inner creation of a carbon-carbon bond (digital simulation). Besides, absence of reductive formation of dimers is a further indication of a preferential intramolecular reactivity determined by the SupLUMO interaction (*cis* isomer pre-organization). The redox-gated covalent bond, serving as electron reservoir, was studied via atropisomerism of the reduction product (VT-NMR study). The overall picture derived from this in-depth study of 2,2'-di(*N*-methylpyrid-4-ylium)-1,1'-biphenyl proves that *trans* and *cis* species are worth considered as intrinsically sharply different, that is, as doubly-electrophoric and singly-superelectrophoric switchable assemblies, beyond conformational isomerism. Most importantly, the through-space-mediated SupLUMO may come in complement of other weak interactions encountered in Supramolecular Chemistry as a tool for the design of electroactive architectures.

Introduction.

To master functional electrons in molecules, there are molecular devices.[1] However, the smaller and more compact they are, the tougher is the implementation of a functional scheme normally suited to multicomponent assemblies.[2] Spatial confining, that pushes multifunctional integration to its limits, is likely to give rise to *emergent behaviors* insofar as intramolecular entanglement of various types of interactions increases complexity, which is regarded as a source for new properties. However, the level of complexity likely to favor occurrence of a functional emergence is highly variable. It spans from that of a mere benzene ring out of which aromaticity arises[3] or from that of simple expanded pyridiniums displaying unusual phenomenon of inversion of electrochemical potentials.[4] It goes up to that of the intricate supramolecular machinery out of which life emerges.[5,6] As a means to approach functional emergence, a molecular design that, for instance, lets some room to serendipity[7–9] can be considered. Here we show that this conception strategy implemented to electron storage within small but conformationally flexible molecular containers, indeed provides a unique opportunity to monitor the process of functional emergence (namely, a sudden change of electronic structure) at a reasonable expense for experimental and theoretical prerequisites. Thus, instrumental for our demonstration, is the notion that certain covalent interactions can be manipulated to overturn the energy penalty originating in electrostatic repulsion[10–12] that results from intramolecular charges (electrons) confining. It's indeed a matter to take advantage of spin pairing energy in order to stabilize electrons to be hosted in the reservoir bond of a semi-rigid electrophoric molecule.[13]

Molecular-level multielectron storage is a challenge for interrelated research topics of artificial photosynthesis and molecular electronics.[14–18] One recent approach towards this goal stems in setting up functional expanded LUMOs that develop through space within purposely designed multi-electrophoric covalent architectures (denoted as super-electrophores)[13],[19] and that are to be filled with electrons to form chemically reversible bonds. It is tantalizing to categorize these inter-electrophoric interactions within the context of supramolecular sciences, envisioning electrochemistry[20] like supramolecular photochemistry,[2] and terming these functional frontier orbitals as “supramolecular” i.e. “supra-MOs” denoted as SupLUMO, SupSOMO or SupHOMO.[13] Scaffold serving as structural platform for spatial layout of redox-active components can be constrained, as is the case for rigid 1,8-disubstituted naphthalene,[13] or only restrained, as is herein the case of semi-rigid biphenyl within 2,2'-di(*N*-methylpyrid-4-ylium)-1,1'-biphenyl labelled **1** (Figure 1A). In the case studies of functional assemblies based

on well-suited pyridinium electrophores,[13] the SupLUMO is anticipated to emerge when there is a symmetry-allowed, out-of-plane, sigma overlap between the $2p_z$ atomic orbitals (AOs) of the two C(γ) atoms also participating in the pi-conjugation of each pyridinium cycle (Figures 1A and 1B). In other words, the SupLUMO construct is foreseen from askew stacking of pyridinium rings such that a through-space overlap of their π* LUMO in a σ way[21] takes place at the C(γ) close contact site (see $\mathbf{1}_{cis}$ in Figure 1A). The so-obtained structure shows a canted layout of the pyridinium cycles with respect to one another, with a distance between the two C(γ) atoms smaller than the sum of their van der Waals radii, that is 1.70 × 2 = 3.40 Å.[22] The point here is that architecture of **1** is such that fitting the criteria for SupLUMO existence is dependent on *trans/cis* conformation, which is the degree of freedom ingredient of the molecular design. In fact, one may even anticipate the unfavorable situation of a prevailing *trans* conformer, based upon inter-pyridinium coulombic repulsion.

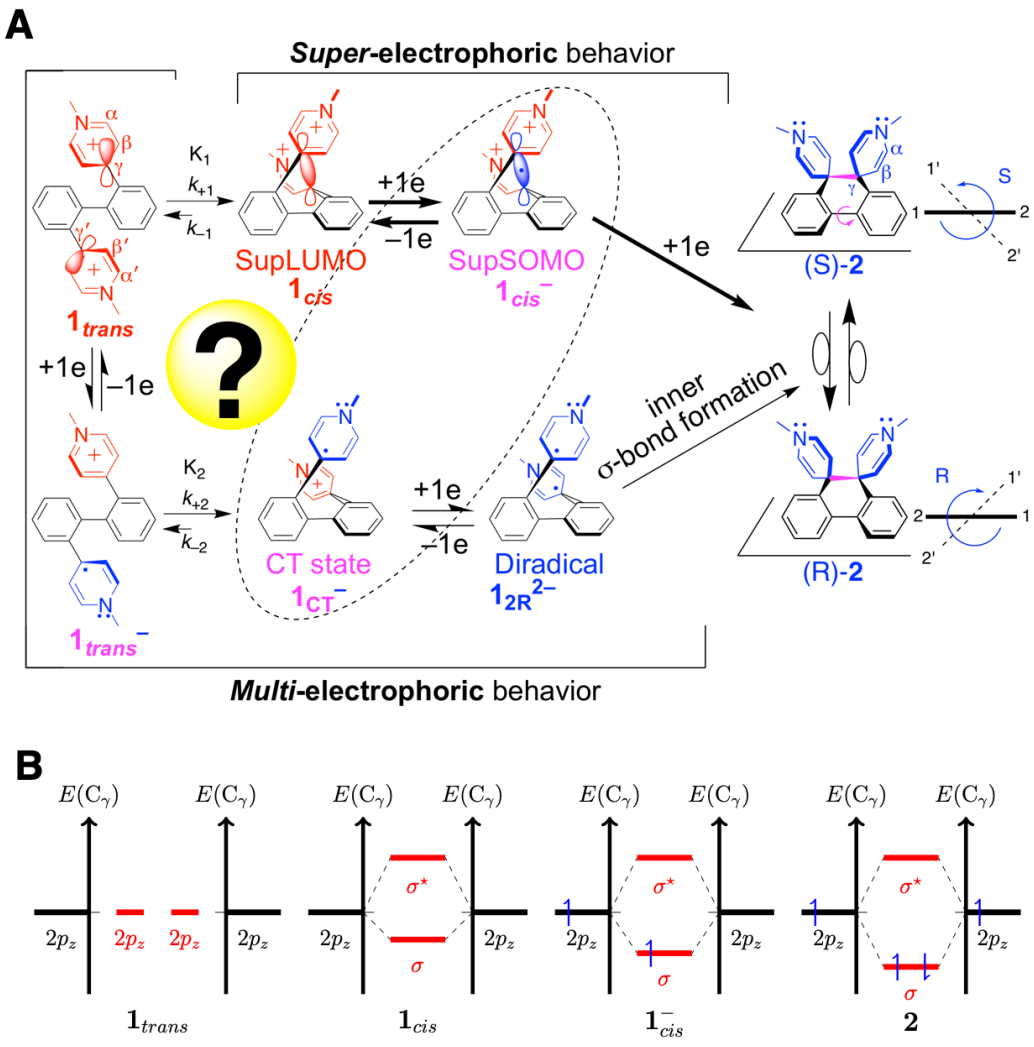

Figure 1. Pictorial representation of two possible mechanistic pathways towards 2 & Energy level diagrams depicting the C(γ)-C(γ) covalent bond formation along the electrochemistry reaction path (delocalized description). (A) Apparent two-electron reduction of **1** into **2**. **2** is the dihydrophenanthrene-like two-electron-reduced product of assembly **1**. **2** exists in the forms of two atropisomers (*S*)-**2** and (*R*)-**2**. Top path: *delocalized* description; bottom path: *localized* description. (B) Conformationally-gated energy gap opening upon "sudden symmetry rising" between $\mathbf{1}_{trans}$ and $\mathbf{1}_{cis}$ and subsequent filling of the SupLUMO of $\mathbf{1}_{cis}$ to store a pair of electrons within **2**.

However, given that we here demonstrate that the only reduction product of **1** is the 9,10-dihydrophenanthrene-like species (**2** in Figure 1A) that is, the intramolecularly σ-bonded species, the question is raised of the identity of the conformer of **1** prevailing in solution. This finding indeed suggests that, unexpectedly, **1** in its native state could be in its *cis* super-electrophoric form, $\mathbf{1}_{cis}$ (Figure 1A), on account of the energy-stabilizing impact of the SupLUMO. Alternatively, the redox-active assembly adopts the *trans* conformation $\mathbf{1}_{trans}$ that behaves as a bi-electrophore (Figure 1A). A structure preparation step for the formation of **2** is therefore required, that could be triggered by a first electron transfer giving a preorganized charge-transfer (CT) state ($\mathbf{1}_{CT}^{-}$ in Figure 1A), followed by a second one-electron reduction and "intramolecular dimerization of pyridinyl radicals" giving **2** (Figure 1A). But the inconvenience of this latter path resides in spurious formation of *inter*-molecular σ-dimers; however, none of these species was experimentally detected. Deciphering pathways between **1** and **2** is a mechanistic issue of paramount importance insofar as it will provide with valuable insights into the very nature of the SupLUMO and its actual impact on both molecular structure (e.g. folding) and reactivity, in particular redox chemistry. Indeed, it's a matter of choosing to adopt a *delocalized* or *localized* description, that is a *super*-electrophoric or a *multi*-electrophoric behavior (Figure 1A), in order to properly describe the reactivity of the functional assembly.

By combining experimental and theoretical approaches, we show that the SupLUMO is an actual energy stabilizing interaction, which is large enough to drive to the pre-organization of the native electrophoric assembly as a super-electrophore ($\mathbf{1}_{cis}$), thus preparing the inner-sphere reductive transformation of **1** into **2**. Also, a clear-cut picture is derived for the SupLUMO-induced upheaval, comprised of a sudden symmetry rising and an abrupt change of electronic structure. This sharp transformation not only makes that $\mathbf{1}_{trans}$ and $\mathbf{1}_{cis}$ are worth considered as different molecular entities beyond conformational isomerism but also, it turns out that this event of synergistic nature gives us the opportunity to thoroughly investigate the *emergence* process. Incidentally, we demonstrate that inversion of standard redox potentials occurring for both reductive bond formation (production of **2**) and oxidative bond cleavage (regeneration of

1) are electrochemical phenomena intrinsic to such a SupMOs-based molecular-level bielectronic storage. Also, atropisomerism of **2** (Figure 1A) enables to investigate the robustness of the electrochemically formed reservoir-bond (SupHOMO), beyond merely evidencing the existence of this elongated covalent linkage.

Results and Discussion.

Crystal (solid) state study.

If a solution of conformers in equilibrium yields crystals, the identity of the most abundant conformer in solution cannot be directly derived from single-crystal X-ray diffraction.[23] However, it happens that the picture derived from solid state accurately reflects actual content of solution. Interestingly, X-ray diffraction of **1**, that is of crystal **1**.2PF_6 (see Figure 2 and Section S2 in Supporting Information), tells us that electrophores adopt the *cis* conformation (denoted $\mathbf{1}_{cis}$) in the solid state instead of the *trans* layout anticipated based upon combined effects of steric hindrance and charge repulsion between cationic pyridinium moieties (Figure 2). Main structural features are the following: interannular torsion angle (θ) inner to biphenyl scaffold amounts to 54.6(3)°, pyridinium rings are positioned roughly parallel although staggered and distance between C(γ) atoms amounts to 3.082(3) Å.

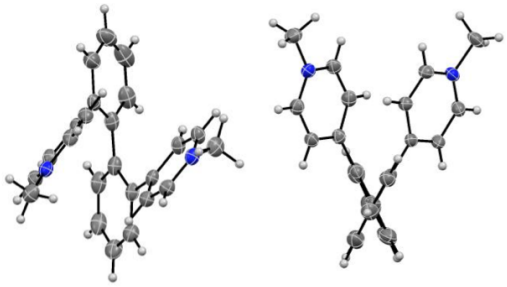

Figure 2. Solid-state study of 1. Single-crystal X-ray crystallography: ORTEP drawings (various views) of molecular structure of $\mathbf{1}_{cis}$ with thermal ellipsoids (40% probability); For clarity reasons, counter anions (PF_6^-) are omitted and only one of the two isomers resulting from axial chirality is shown.

Of note, in the case of dicationic 2,2'-substituted 1,1'-biphenyl scaffold with 9-acridinium[24] as dibenzoannulated pyridinium electron-acceptor subunit, single-crystal X-ray crystallography establishes a similar proximal layout of the electrophoric units (here referred to as a *cis* conformation) with a distance separating carbenium atoms smaller than the sum of their van der Waals radii (3.40 Å)

Solution studies.

First, **1**.2PF_6 was chemically reduced (Na/Hg (5% wt.), $E^{0'} = -1.95$ V vs SCE;[25] CD_3CN) and transformation reaction was monitored by ^1H and ^{13}C NMR (Figure 3A and Section S5 in Supporting Information). The spectrum of the reduction product (**2**) presents well-defined resonance peaks corresponding to the aromatic protons (from the dihydrophenanthrene moiety), thereby demonstrating the diamagnetic nature of the species resulting from reduction (no mono- nor bi-radical species, such as $\mathbf{1}_{cis}^{-}$, $\mathbf{1}_{CT}^{-}$ or $\mathbf{1}_{2R}^{2-}$ in Figure 1A, are detected). Protons doublets α and β of the pyridinium subunits have their chemical shifts significantly modified upon formation of **2**. Loss of aromaticity of pyridiniums subsequent to reduction is responsible for this important difference. In addition, at 298 K, signals of these up-field shifted protons are very broad and split ($\Delta\delta_{H\alpha,\alpha'}$ = 2.00 and 2.50 ppm and $\Delta\delta_{H\beta,\beta'}$ = 3.00 et 3.50 ppm; Figure 3A). This phenomenon is indicative of an exchange regime between the two conformations of the molecule that occurs on the NMR timescale. Indeed, **2** presents two stereoisomers of conformation resulting from the constrained rotation around the interannular bond of biphenyl and of the newly formed bond; these are atropisomers (*S*)-**2** and (*R*)-**2** (see Figure 1A). As observed previously for ^{13}C NMR of naphthalene-based superelectrophore,[13] the C(γ) signal undergoes a huge displacement upon reduction (up-field shifting). The change in hybridization ($sp^2 \rightarrow sp^3$) explains this difference $\Delta\delta_{C\gamma,\gamma'}$ of 109.1 ppm between **1** and **2** (see Figure S9 in Supporting Information). As is the case for related protons, it is noted that room temperature signals corresponding to α and β carbon atoms are barely visible due to the intermediate exchange rate between the two atropisomers (see Figure 3B and Figure S9 in Supporting Information). Last, it is worth emphasizing the cleanliness of the reduction reaction: the formation of by-products such as α-α intermolecular σ-dimers,[26] is indeed not observed despite the rather high concentration (10^{-2} M) of the reaction medium (Figure 3A). This is a second indication that native electrophore (**1**) might be pre-organized in solution for the reduction step ($\mathbf{1}_{cis}$ superelectrophoric behavior in Figure 1). Thus, concerning **1**, although ^1H NMR spectrum of one conformer in its pure form cannot be obtained owing to fast conformational equilibrium, averaged experimental spectrum remains however weighted by respective populations of $\mathbf{1}_{trans}$ and $\mathbf{1}_{cis}$. Interestingly, NOE experiments combined with structural data collected from X-ray diffraction ($\mathbf{1}_{cis}$; Figure 2) and from molecular modeling (optimized geometries of $\mathbf{1}_{trans}$ and $\mathbf{1}_{cis}$; see below), allow identifying a weak correlation specific to $\mathbf{1}_{cis}$ that involves H_β and $H_{5'}$ of distant phenyl (see Section S3 in Supporting Information). This observation substantiates significant abundance of at least 50% for $\mathbf{1}_{cis}$ superelectrophoric conformer in solution.

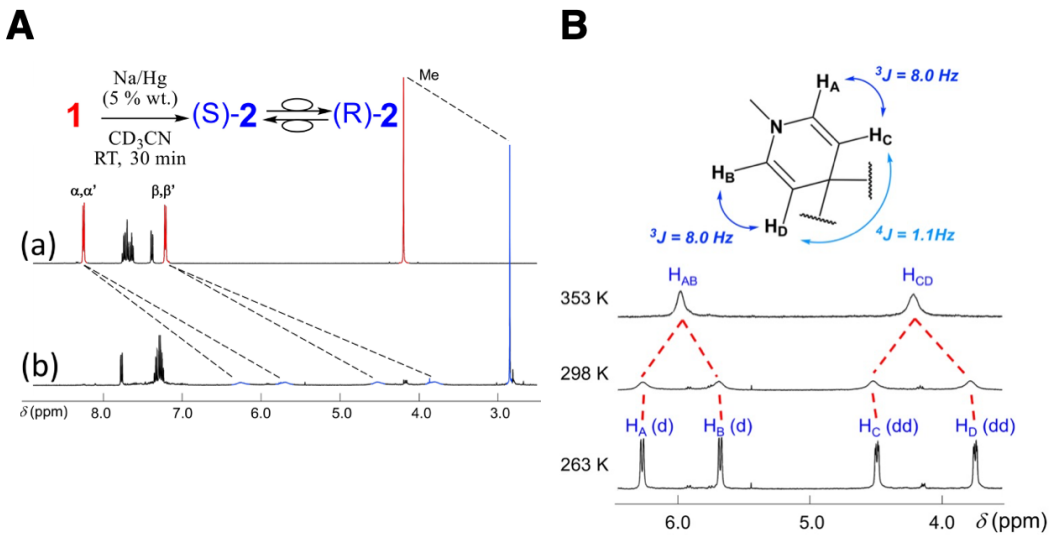

Figure 3. Solution NMR characterization of the reduction product 2. (A) ^{1}H NMR spectra (400 MHz, CD_3CN, 298 K) of **1**.2PF_6 (10^{-2} M) before (a) and after (b) chemical reduction, showing the diagnostic chemical shift of the H(α,α′), H(β,β′) protons of the electrophoric subunits along with their resonance broadening *at room temperature*; refer to labelling scheme in Figure 1A. (B) ^{1}H NMR spectra corresponding to fast, intermediate and slow exchange regimes observed for H(α,α′), H(β,β′) protons of the reduction product of **1**, that is, **2**. Coupling diagram of the model used for the parameters of the simulation. See also Section S6 in Supporting Information.

As regards **2**, the exchange phenomenon was studied by ^{1}H NMR at variable temperature (VT-NMR; see Section S6 in Supporting Information).[27] The rate constants of this exchange were estimated at different temperatures (by simulation of spectra), and the thermodynamic parameters ($\Delta G^{\neq}$, $\Delta H^{\neq}$ and $\Delta S^{\neq}$) associated with the energy barrier of interconversion between the two atropisomers (*S* and *R;* Figure 1A) were determined (see Figure S12 in Supporting Information). At 298 K, the exchange rate is estimated to amount between 100 and 250 s^{-1}, as expected from the broadening of signals ascribed to H(α) and H(β). At the lowest temperature studied (263 K), the two signals corresponding to protons α and α' appear in the form of two doublets (^{3}J = 8.0 Hz), whereas the signals corresponding to protons β and β' are in the form of doublets of doublets (^{3}J = 8.0 Hz and ^{4}J = 1.0 Hz; see Figure 3B). At this temperature, the very weak exchange (slow rate) makes it possible to determine the simulation parameters in static conditions. Thus, for **2**, it was found that activation energy $\Delta G^{\neq}$ = 14.51 ± 0.23 kcal mol^{-1}, with $\Delta H^{\neq}$ = 12.43 kcal mol^{-1} and $\Delta S^{\neq}$ = –7.47 cal mol^{-1} K^{-1}. Electronic structure computations (PBE0-D3(BJ)/def2-QZVPP) accurately reproduce these thermochemical quantities at 263 K: $\Delta G^{\neq}$ = 14.16 kcal mol^{-1}, with $\Delta H^{\neq}$ = 12.80 kcal mol^{-1} and $\Delta S^{\neq}$ = –5.18 cal mol^{-1} K^{-1} (see Section S7 in Supporting Information). The negative value of entropy variation is explained by the fact that transition state between atropisomers (*S*)-**2** and (*R*)-**2** (of C_2 symmetry) is of higher symmetry

(C_{2v}) (see Figure S13 in Supporting Information). Brought together with VT-NMR study of the Na/Hg reduction product, these findings definitively confirm the identity of **2** as a 9,10-dihydrophenanthene (DHP) derivative, hence the number of exchanged electrons: $n = 2$ (see Figure 1A). Of note, in the affiliated conceptual contexts[28] of molecular-level "dynamic redox systems"[29] and of "ultralong C-C bond expandability",[30] two-electron reduction of the sterically demanding bis-acridinium analogue of **1** also yields a DHP derivative, which has been characterized by single-crystal X-ray diffraction.[31,32]

Second, **1**.2PF_6 was electrochemically reduced and the formation of the reaction product was monitored by UV-vis-NIR spectrophotometry (see Figure 4A and Section S8 in Supporting Information). Electronic absorption spectrum of **1**.2PF_6 in solution in CH_3CN (plus supporting electrolyte) shows two bands of equivalent absorbance at 239 and 292 nm. In the course of the reduction process, with the formation of **2**, these two bands decrease to give way to a new band at 265 nm, which is accompanied with a shoulder noticed at 299 nm. No intermediate radical cation of **1**, could be detected in the visible-NIR spectral domain although 1-methyl-4-phenylpyridinyl chromophoric fragment is a potent probe[4b,33,34] (see Figure S17 in Supporting Information). The presence of three isosbestic points (235, 255 and 280 nm) demonstrates a clean and direct reductive conversion of **1** into **2**. Furthermore, **2** is cleanly converted back to **1** upon oxidation at proper potential (see Figure S15 in Supporting Information). Beyond chemical reversibility, it is worth emphasizing, again, the cleanliness of the transformation that suggests that no side reaction such as intermolecular σ-dimerization at α sites occurs, as could reasonably be expected for **1** in its *trans* conformation (i.e. for $\mathbf{1}_{trans}$). Such a lack of –intermolecular– reactivity is reminiscent of that observed in the case of pre-organizing naphthalene scaffold,[13] which was explained by the presence of the SupLUMO diverting the whole reactivity. De facto this observation puts forward, once again, pre-organization of electrophoric components that is, presence of $\mathbf{1}_{cis}$ in solution. Notwithstanding this evidence, as to whether reaction of the less abundant conformer (say *cis*) could be kinetically favored as compared to the major one (e.g. *trans*) under the principle of Curtin-Hammett control,[35] is not a relevant issue in the present case study. Indeed, σ-bond formation (whether inter- or intra-molecular) is a barrierless process (see also below: energy profile study and Figure 7A) such that this type of kinetic control does not apply here. On the other hand, as far as electrochemistry is concerned, electric field within double-layer of working electrode during reduction may be impactful on *trans*/*cis* ratio, by locally inducing the conformation with cationic pyridiniums pointing in the same direction, thereby energetically favoring the *cis* superelectrophoric isomer.

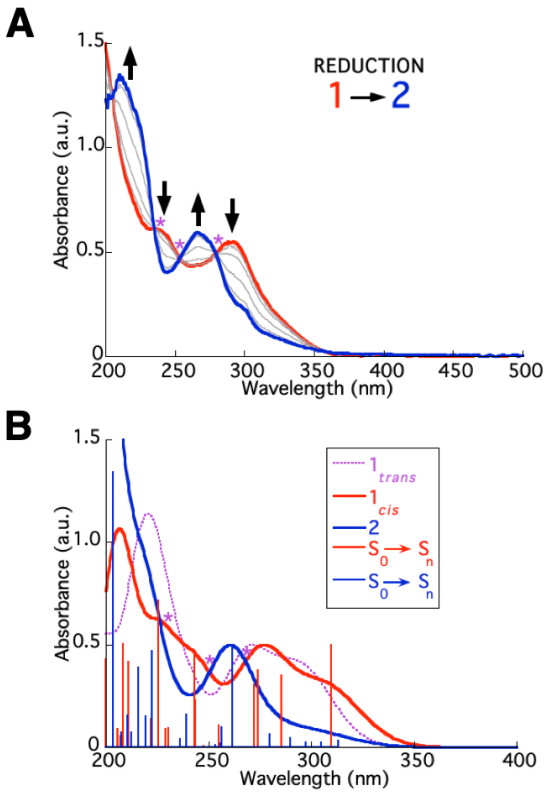

Figure 4. Electronic properties. (A) UV-vis spectroelectrochemistry experiment of a solution of **1** (red trace) in CH_3CN ($c = 5.6 \times 10^{-4}$ M with 0.1 M of $TBAPF_6$). The spectrum of **2** (blue trace) is obtained after the application of a negative potential (−1.4 V vs Ag/AgCl) using a Pt grid as the working electrode. Asterisks (*) indicate isosbestic points. (B) Computed absorption spectra of $\mathbf{1}_{trans}$ (violet, broken line), $\mathbf{1}_{cis}$ (in red) and **2** (in blue) in CH_3CN along with S_0–S_n electronic vertical transitions for $\mathbf{1}_{cis}$ and **2**. Intensities are normalized to 0.5 with respect to the red-edge bands.

At this stage it is worth tapping into resources of molecular modeling to get comprehensive insights into electronic structure that underpins optical properties of $\mathbf{1}_{trans}$ /$\mathbf{1}_{cis}$ and **2**. A structure optimization (see Figure 5A) at density-functional theory (DFT) level according to the *DHthermo* protocol[36] (PBE-QIDH/DH-SVPD) was performed using a continuum representation of the solvent (here CH_3CN) and upon naturally starting from the *trans* conformation of **1**, that is $\mathbf{1}_{trans}$ (see Figures 1A, 5A and 5B). Interannular torsion angle of biphenyl scaffold, θ, was found to actually amount to 125.7°. Then, electrons were added step-wisely, firstly giving $\mathbf{1}_{trans}^{-}$ (one-electron "vertical" reduction), which was found to relax (torsional motion) into $\mathbf{1}_{cis}^{-}$ / $\mathbf{1}_{CT}^{-}$ ($\theta = 48.4°$; Figures 1A and 5B), and next the two-electron-reduced species, which was found to relax into distorted 9,10-dispiro(*N*-methyl-1,4-dihydropyridin-4-yl)dihydrophenanthrene derivative **2** (θ = 21.1°; Figures 1A and 5B),

featuring an additional –elongated– bond linking the two sterically crowded C(γ) atoms. Further exploration of the potential energy surface (PES) went through stepwise oxidation of **2** (one-electron removal) to recover $\mathbf{1}_{cis}^{-}$ (formally $\mathbf{2}^{+}$). Subsequent one-electron oxidation to formally give $\mathbf{2}^{2+}$ did not led to the recovering of starting geometry ($\mathbf{1}_{trans}$) but to a new minimum in the PES corresponding to a pre-organized *cis* conformer of native superelectrophore $\mathbf{1}_{cis}$ ($\theta = 57.2°$; see Figures 1A, 5A and 5B) that closely resembles the molecular structure found in the solid state (Figure 2). Once the PESs of native, singly- and doubly-reduced electrophore were mapped (Figure 5A), time-dependent DFT (TD-DFT) computations (PBE-QIDH/cc-pVTZ) of the electronic spectra of $\mathbf{1}_{trans}$, $\mathbf{1}_{cis}$, $\mathbf{1}_{cis}^{-}$ and **2** were performed for comparison purposes with UV-vis-NIR spectroelectrochemical (SEC) data (Figure 4A). From this assessment (Figure 4B; see also Figure S16 in Supporting Information) it clearly follows that the features of native electrophore in solution are essentially those of the *cis* conformer $\mathbf{1}_{cis}$. The strong charge-transfer character of the first computed transition (HOMO–SupLUMO; Figure 5C) induces at TD-DFT level a slight underestimation (/overestimation) of its energy (/intensity) with respect to experiment.[37] On the other hand, there is a mismatch between SEC data for **1** and calculated spectrum of $\mathbf{1}_{trans}$. In terms or relative abundances of conformers *trans*/*cis*, this finding is again unambiguously consistent with a prevailing *cis* superelectrophore. Besides, upon examination of frontier MOs (Figure 5C), one can derive a first striking feature, which is that the LUMO is *located* over the two pyridinium components *separately* within $\mathbf{1}_{trans}$ (*bielectrophoric* behavior, Figure 1A) whereas the LUMO of $\mathbf{1}_{cis}$ *encompasses* the two pyridinium units by *continuously* expanding through space between the two C(γ) (*superelectrophoric* behavior, Figure 1A). We refer to this latter *delocalized* bonding MO as a SupLUMO, which is a diagnostic feature of the synergistic interplay of redox-active components.[13] In fact, distance between C(γ) atoms of neighboring pyridiniums decreases from 4.753 Å within $\mathbf{1}_{trans}$ to 3.120 Å within $\mathbf{1}_{cis}$, thus imposing a nearly co-facial conformation of both pyridinium rings. Under these conditions, the sigma overlap between the two $2p_z$ C(γ) AOs is symmetry-allowed. It follows that added electron within $\mathbf{1}_{cis}^{-}$ is *delocalized* over both electrophoric components (SupSOMO; *d*(Cγ–Cγ') = 2.712 Å). In other words, the charge-transfer picture between one singly-reduced pyridinium and the other pyridinium in its native state ($\mathbf{1}_{CT}^{-}$ bielectrophoric behavior in Figure 1A) is not relevant. This also means that regardless of whether the first electron is initially transferred to the *trans* or *cis* isomers, the same intermediate reduction product is formed: $\mathbf{1}_{cis}^{-}$, such that the superelectrophoric pathway only is borrowed for second reduction to yield **2** (the diradical species $\mathbf{1}_{2R}^{2-}$ in Figure 1, does not exist). Within **2**, *d*(Cγ–Cγ') amounts to 1.580 Å, that is, an

elongated C-C covalent bond as compared to C-C bond-length calculated at the same level of theory for ethane (1.520 Å), which is not sterically constrained contrary to the case of **2**. A second salient feature has to do with the HOMO of **2**, actually worth referred to as the SupHOMO of the two-electron-reduced superelectrophore. This latter, which is comprised of the newly-formed bond, roughly has the same spatial expanse as that of SupLUMO within $\mathbf{1}_{cis}$ (Figure 5C). This means that electron loading and retrieval take place at the same location within superelectrophore, the SupLUMO of $\mathbf{1}_{cis}$ thereby functioning as a genuine (empty) electron reservoir (and SupHOMO of **2** serving as the filled reservoir).

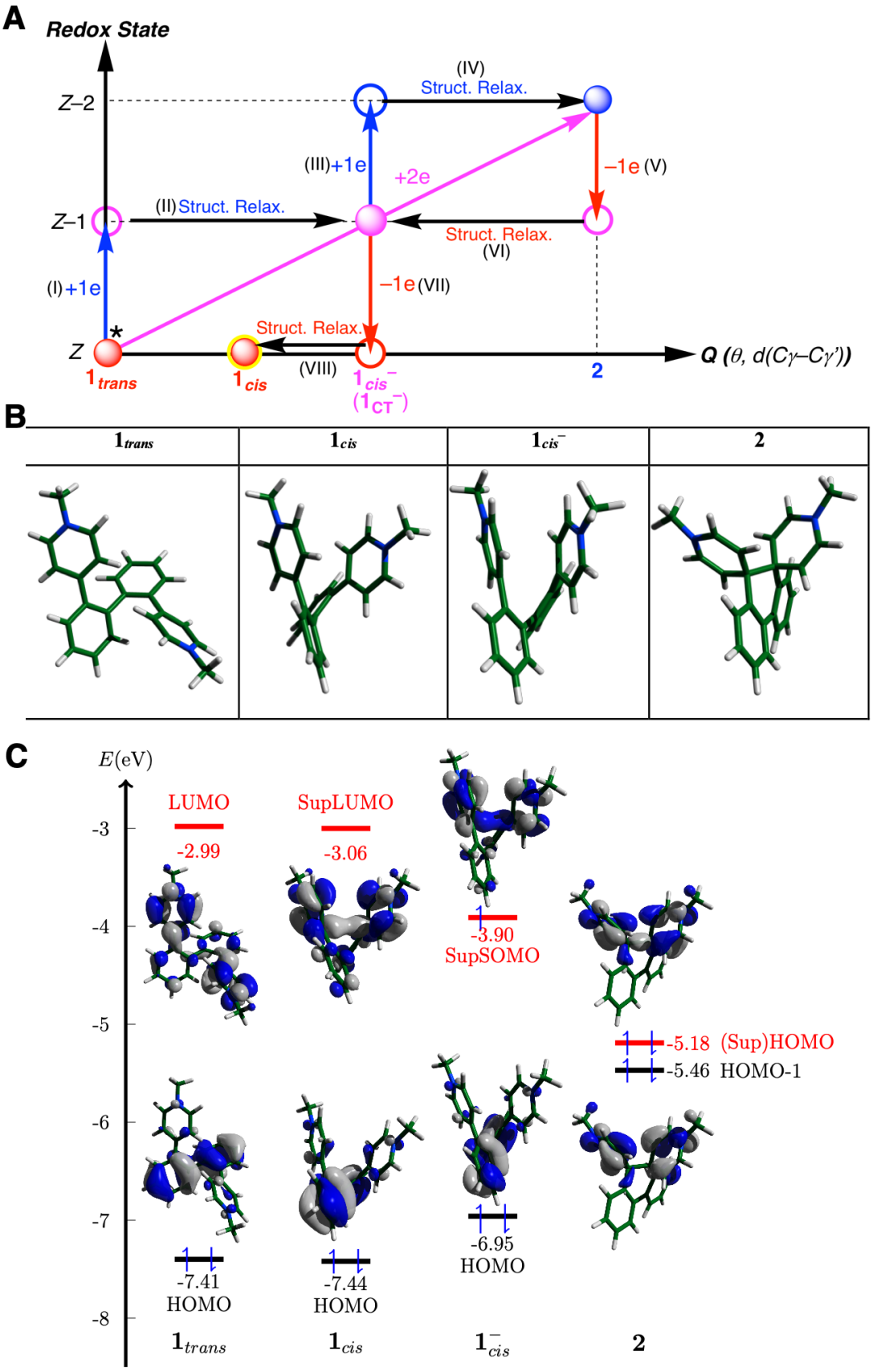

Figure 5. Molecular modeling. (A) Perfecting the computational procedure (8-step geometry optimization) for **1** and **2**. Coordinate *Q* represents the structural folding of the superelectrophore for a given redox state. Closed

circles indicate optimized structures obtained from $\mathbf{1}_{trans}$ upon electron addition (blue arrows) or derived from **2** upon electron retrieval (red arrows), whereas open circles denote unoptimized geometries that are followed by structural relaxation (black arrows). Asterisk (*) indicates the starting geometry of optimization process. (B) Optimized molecular geometries of $\mathbf{1}_{trans}$, $\mathbf{1}_{cis}$, $\mathbf{1}_{cis}^{-}$ and **2**. (C) Frontier MOs of $\mathbf{1}_{trans}$, $\mathbf{1}_{cis}$, $\mathbf{1}_{cis}^{-}$ and **2** along with their energy; iso-contour value of 0.02.

Experimentally, cyclic voltammetry of **1** enables full electrochemical characterization of this reservoir-bond. Regardless of scan rate, cyclic voltammograms (CVs) disclose two electrochemically irreversible processes (Red-1 and Ox-2; see Figure 6A) indicative of intervening electrochemical-chemical (EC) mechanism. Evidenced electrochemical hysteresis (ΔE_{Hyster} in Figure 6A) is typically delineated by cathodic peak at $E_{\text{pc-(Red-1)}} = -1.07$ V and anodic peak at $E_{\text{pa-(Ox-2)}} = +0.03$ V, which respectively correspond to reductive formation and oxidative cleavage of the reservoir bond within superelectrophore as a bistable system. One shows that (i) the reduction peak (Red-1) relates back to a two-electron process (Figure 6)[38] and (ii), inversion of potential is demonstrated for the reduction regime. Indeed, not only semi-integration of the voltammetric reduction wave yields a neo-polarogram of a well-defined shape, indicating that electron transfers are fast and correlated (see Figure S20 in Supporting Information), but also subsequent log-plot analysis of this semi-integrated neo-polarogram gives a straight line (Figure 6B).[39] This outcome is consistent with an inversion of standard potentials (ΔE^0) of large magnitude, as confirmed by digital simulation of a set of CVs that establishes $E^0_1 = -1.13$ V and $E^0_2 = -0.76$ V that is, $\Delta E^0 = 370$ mV (see Section S11 in Supporting Information). This is in line with the potential inversion of 390 mV calculated for two-electron reduction of $\mathbf{1}_{cis}$ (see Section S12 in Supporting Information). Digital simulation of CVs also indicates that potential inversion is at work for oxidative cleavage of the reservoir bond ($\Delta E^0 = 210$ mV). Most importantly, this simulation substantiates the EEC (forward, reduction) – EEC (backward, oxidation) electrochemical mechanism of σ-bond formation/cleavage cycling (see Chart S1 in Section S11 of Supporting Information). This intra-molecular process is further corroborated on establishing the direct proof of the absence of σ-dimer formation (inter-molecular process) by performing an electrochemical study as a function of concentration of native electrophore **1**. Thus, it is found that reduction potential does not shift towards less negative values upon increasing concentration of **1** and that electrochemical irreversibility of CVs is independent from this concentration (see Section S13 in Supporting Information).[40,41] It is worth noting that, within $\mathbf{1}_{cis}^{-}$, short-lifetime unpaired electron is buried within the SupSOMO and cannot get involved into outer-sphere intermolecular processes, conversely to hypothetical $\mathbf{1}_{CT}^{-}$ (Figure 1), thereby proving that this latter does not exist.

Brought together, these insights confirm that delocalized pathway relying on superelectrophoric behavior is operative, with $\mathbf{1}_{cis}$ and above all $\mathbf{1}_{cis}^{-}$ as embodiments (Figure 1A). A special emphasis is put on the fact that evidenced electron correlation, reflected by phenomenon of potential inversion, is sole consistent with intervening SupSOMO.

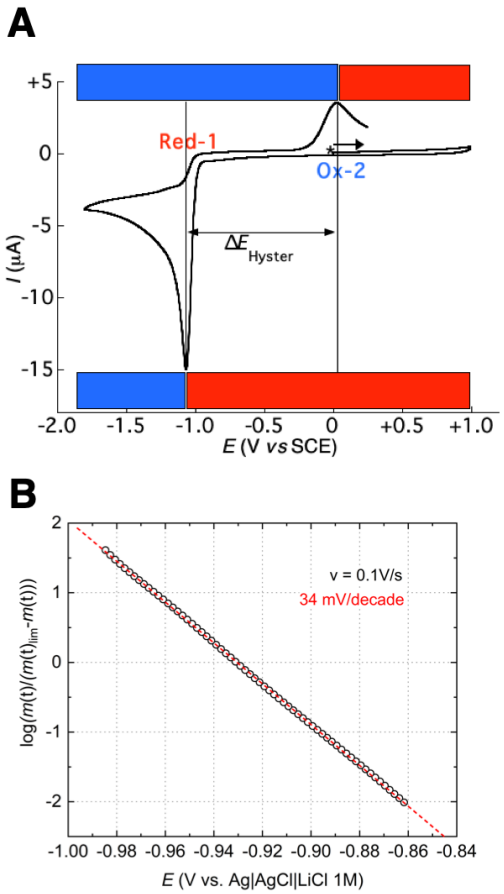

Figure 6. Electrochemical behavior. (A) Cyclic voltammetry experiment of **1**.2PF$_6$ (c ≈ 5 × 10^{-4} M in CH$_3$CN with 0.1 M of TBAPF$_6$, Platinum electrode) recorded at scan rate *v* of 0.1 V s^{-1} (see Ref. [38]). Asterisk (and arrow) indicate the starting potential (and direction) of the scan. Red and blue zones indicate dominant species in solution: **1** and **2**, respectively. (B) Log–plot analysis of semi-integrated neo-polarogram (Figure S20 in Supporting Information) calculated for the reduction step (5.2 × 10^{-4} M **1**.2PF$_6$ and TBAPF$_6$ 0.1 M in CH$_3$CN, glassy carbon electrode, scan rate 0.1 V s^{-1}) giving only one slope equal to 34 mV/decade.

These findings are in line with outcomes of UV-vis-NIR SEC that show apparent direct transformation of $\mathbf{1}_{cis}$ into **2** without observation of intermediate $\mathbf{1}_{cis}^{-}$ (nor $\mathbf{1}_{trans}^{-}$)[33] absorbing in the visible-NIR domain (see Figure S14 in Supporting Information), which cannot accumulate since second one-electron reduction (E^0_2) is energetically less demanding than the first one-electron reduction (E^0_1) because of potential inversion. On the other hand, chemical step is essentially ascribed to electro-structural relaxation (tetrahedralization of C(γ) atoms due to hybridization change from sp^2 to sp^3) that occurs upon second electron transfer and ends up

with formation of spiro C(γ) atoms (see Figure 5B). This significant relaxation accounts for inversion of standard electrochemical potentials[10,13] (electro-structural relaxation also occurs during first one-electron reduction, but to a much lesser extent; see Figures 5B and 7A). The overall picture we get of the SupLUMO points out its critical functional role at the core of superelectrophore, spanning from merely arranging the *3D* structure of the native state ($\mathbf{1}_{cis}$ versus $\mathbf{1}_{trans}$) to determination of reactivity with respect to electron transfers (including potential inversion) and to storage. With these mechanistic insights in mind, a further clarifying of SupLUMO emergence goes through a study of the energy profile of various key species.

Energy profile study: evidencing SupLUMO emergence.

From a computational standpoint, torsional degree of freedom inner to biphenyl scaffold (θ) provides a means for mapping the PES of the electrophoric assembly in its various redox states [*Z*]: native ([*Z*] = 2+), singly-reduced ([*Z*] = 1+) and doubly-reduced ([*Z*] = 0). Incremental variation of θ starts from the optimized geometry of $\mathbf{1}_{trans}$ (see Figure 7A).

The striking feature disclosed by diagram of Figure 7A is the virtually vertical transition (otherwise worth referred to as a change of electronic structure) that occurs within one degree only, between torsion angles (θ) amounting to 68.8° and 67.8° ([*Z*] = 2+). This range corresponds to a *d*(Cγ–Cγ') distance decrease by 18.5%, from 4.003 Å to 3.263 Å, falling below the critical sum of the van der Waals radii of carbon atoms (3.40 Å). Whilst pyridinium rings are pivoting by ca. 20° (tilt angles of ca. 45° with respect to phenyl rings are reached) and are becoming almost cofacial, sigma overlapping of $2p_z$ gets optimized (see Figure 7B). This is a "*sudden symmetry rising*" (SSR). Concomitantly, for the singly-reduced superelectrophore ([*Z*] = 1+), spin density originally located over one of the two pyridiniums before SupSOMO arises, becomes delocalized over both of them afterwards (Figure 7B).[42] This sharp transition allows visualizing a *functional emergence*: namely that of a novel electronic structure, which involves SupLUMO for [*Z*] = 2+, SupSOMO for [*Z*] = 1+ and SupHOMO for [*Z*] = 0. Interestingly, for electrophore in its native state, Figure 7A also reveals that $\mathbf{1}_{cis}$ is slightly more stable than $\mathbf{1}_{trans}$ by 0.12 eV i.e. 2.65 kcal mol^{-1} (energy barrier between $\mathbf{1}_{trans}$ and $\mathbf{1}_{cis}$ amounts to ca. +0.39 eV i.e. +9.09 kcal mol^{-1}, consistent with above-mentioned fast *trans*/*cis* equilibration at NMR timescale). Equilibrium constant K_1 (see Figure 1) is roughly estimated to amount to 88 corresponding to $\mathbf{1}_{cis}$ virtually pure in solution (98.9 %). This agrees with UV-vis SEC and electrochemical analyses but shows a marked difference with the rough assessment derived

from NOE-NMR, giving an abundance of at least 50% only. Whatever, the point is that $\mathbf{1}_{cis}$ is the prevalent species in solution even if its abundance could not be determined with precision. Besides, on examining the [*Z*] = +1 energy profile, it is also noteworthy that elusive $\mathbf{1}_{cis}^{\bullet}$ species hosting the SupSOMO is a global minimum that allows figuring out the relaxation process of $\mathbf{1}_{trans}^{\bullet}$ to $\mathbf{1}_{cis}^{\bullet}$, which shunts the localized pathway (multielectrophoric behavior) of reduction to the benefit of the delocalized pathway (superelectrophoric behavior).

All in all, the stabilization of $\mathbf{1}_{cis}$ is unambiguously ascribed to intervening SupLUMO. Cross involvement of $2p_z$ AO of C(γ) in both the π-conjugated system of pyridiniums and in the through-space overlap of energy-degenerate $2p_z$ orbitals of vicinal C(γ) atoms makes that, even though empty, the SupLUMO does globally impact on the energy (and electronic structure) of $\mathbf{1}_{cis}$, which is found to be energy-stabilized (see Figure 7A).[43] In addition, as can be seen on the diagram, there is no energy barrier to overcome in going from $\mathbf{1}_{cis}$ to $\mathbf{1}_{cis}^{\bullet}$ to **2** but only electro-structural relaxation processes as driving forces. This outcome is in line with experimentally and theoretically evidenced inversion of standard potentials of first and second one-electron reductions in electrochemistry.

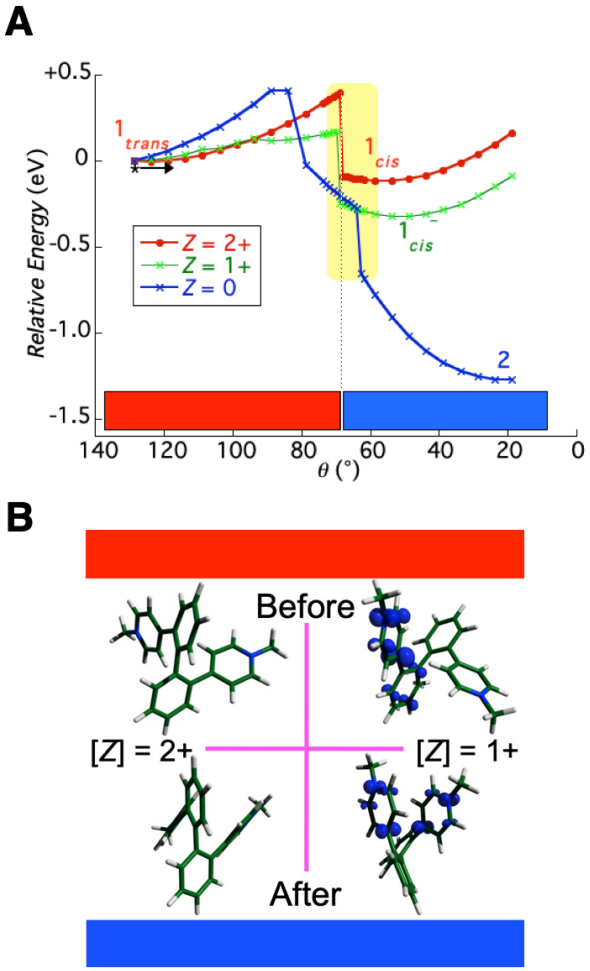

Figure 7. Visualizing SupLUMO emergence along with "sudden symmetry rising" (SSR). (A) Exploring the PES of superelectrophore in redox states [*Z*] = 2+, 1+, 0: energy rotation profile, with respect to the θ torsion angle (PBE0-D3(BJ)/def2-SVP); See also Ref. [44]; Asterisk (and arrow) indicate the starting point of geometry optimization. (B) Optimized geometries computed at either side (i.e. right before and right after) of SSR transition for (i) **1** ([*Z*] = 2+) showing electro-structural reorganization (pivoting of pyridinium rings) that accompanies SupLUMO emergence and (ii), **1** ([*Z*] = 1+) showing electro-structural reorganization together with spin density redistribution that accompanies SupSOMO emergence. Red and blue zones indicate electronic affiliation of redox-active species that correspond to *localized* versus *delocalized* descriptions, respectively.

Conclusion.

A chemist naturally pictures molecule **1** in its *trans* conformation $\mathbf{1}_{trans}$, which is also the starting point for geometry optimization (Figures 5A and 7A). However, the *cis* species $\mathbf{1}_{cis}$ is the global minimum for superelectrophore in its native state. This counter-intuitive finding is explained by existence of SupLUMO energy-stabilizing interaction inner to $\mathbf{1}_{cis}$.

On the one hand, when prevalent $\mathbf{1}_{cis}$ species is reduced, it borrows the superelectrophoric pathway (SupLUMO/SupSOMO/SupHOMO) towards **2**. On the other hand, when $\mathbf{1}_{trans}$ is reduced: the one-electron-reduced species (transient $\mathbf{1}_{trans}^{-}$) readily relaxes into $\mathbf{1}_{cis}^{-}$, which belongs to the superelectrophoric pathway, thereby shunting the multi/bi-electrophoric path. In both cases, reduction goes through $\mathbf{1}_{cis}^{-}$: an elusive species (because of inversion of electrochemical potentials) that partakes to superelectrophoric pathway (Figure 1A).

This somewhat unexpected result draws attention on conjectures related to conformational features of multicomponent assemblies especially when electroactive functional units are involved. In the present case, we evidence a novel driving force for the reaction taking place under certain energy and symmetry criteria, which relies on sudden energy stabilization and fusion of the LUMOs of two electrophilic centers [i.e. C(γ)], featuring a through-space expansion of emerging SupLUMO. Although covalent in nature, this directional stabilizing interaction may come in complement to well-known weak noncovalent interactions such as hydrogen bonding, aromatic interactions (ion-pi interplay, pi-pi stacking), hydrophobic association, electrostatic interactions and van der Waals forces encountered in Supramolecular Chemistry.

Even if $\mathbf{1}_{cis}$ and $\mathbf{1}_{trans}$ are formally conformers, $\mathbf{1}_{cis}$ is more closely affiliated to **2** than to $\mathbf{1}_{trans}$ from the standpoint of electronic structures, owing to existence of the SupLUMO as bonding interaction. $\mathbf{1}_{cis}$ is actually worth referred to as the $\mathbf{2}^{2+}$ native form of **2** (blue zone in Figure 7A).

Insofar as bond formation within superelectrophore results from mere filling of pre-existing bonding MO, namely the SupLUMO, and that second one-electron reduction is assisted by structural relaxation (hybridization change) resulting in potential inversion, this latter phenomenon together with electrochemical hysteresis, are worth viewed as features of electron-reservoir bonds relying on SupLUMOs.

Our results feed the discussion on the true nature of conformers in certain particular cases of compact multifunctional small molecules. Here, electronic-structure sharp transition associated with "sudden symmetry rising" are constitutive of the *functional emergence* embodied by the *SupLUMO*. This event delineates switching from a *localized* description of electrophoric components within assembly $\mathbf{1}_{trans}$ (red zone in Figure 7A) to a *delocalized* description of both pyridinium subunits that form a made-in-one-piece electronic entity, integral part of molecule $\mathbf{1}_{cis}$ (blue zone in Figure 7A).

Experimental Section.

Single-crystal X-ray crystallography.

A single crystal of **1** was selected, mounted onto a MiTeGen cryoloop and transferred into a cold nitrogen gas stream. Intensity data were collected with a Bruker Kappa APEX-II CCD diffractometer using a micro-focused Cu-Kα radiation (λ = 1.54178 Å). Data collection was performed at 200 K, with the Bruker APEXIII[45] suite. Unit-cell parameters determination, integration and data reduction were carried out with SAINT[45] program. SADABS[46] was used for scaling and absorption corrections. The structure was solved with SHELXT[47] and refined by full-matrix least-squares methods with SHELXL[48] using Olex2 software package.[49] All non-hydrogen atoms were refined anisotropically. Deposition Number 2081294 contains the supplementary crystallographic data for this paper. These data are provided free of charge by the joint Cambridge Crystallographic Data Centre and Fachinformationszentrum Karlsruhe Access Structures service.

(Variable-Temperature) NMR experiments.

^{1}H NMR and ^{13}C NMR spectra were recorded at 400 MHz, on a Bruker Avance III 400 spectrometer for variable temperature experiments, and also at 600 MHz, on a Bruker Avance III 600 spectrometer at 298 K for NOE experiments. Chemical shifts for ^{1}H NMR spectra are referenced relative to residual protium in the deuterated solvent (CD_3CN δ = 1.94 ppm). Chemical shifts for ^{13}C NMR spectra are referenced relative to carbon in the deuterated solvent

(CD_3CN δ = 118.28 and 1.32 ppm). When needed, NMR assignments were determined by bidimensional NMR experiments (COSY, HSQC, HMBC and NOESY).

The NUMARIT algorithm via the SpinWorks software,[50] was used for the whole VT-NMR simulation.

UV-vis-NIR spectroelectrochemistry.

Spectroelectrochemistry was performed using an optically transparent thin-layer electrode cell with a three-electrode system (Ag/AgCl reference electrode) mounted in a thin layer (thickness 0.18 mm) between CaF_2 optical windows. Sufficiently optically transparent platinum gauze (80 mesh) of the size 5 × 5 mm served as the working electrode. The Ag-wire served as a quasireference electrode (+0.35 V against Fc^+/Fc). The potential scan rate was 0.005 V s^{-1}. Spectral changes in the course of potential scanning were registered using Agilent 8453 diode-array UV-vis-NIR spectrometer. The absorption spectra were recorded against the blank solution of 0.1 M tetrabutylammonium hexafluorophosphate ($TBAPF_6$) in acetonitrile (anhydrous, 99.8%, Sigma-Aldrich, Germany). $TBAPF_6$, which was used as supporting electrolyte, was obtained from Sigma-Aldrich and was dried before the use.

Molecular electrochemistry.

Cyclic voltammetry (CV) experiments were performed at 298 K using 5×10^{-4} M of **1** in Ar-purged MeCN (Aldrich, anhydrous, 99.8%) solutions with 0.1 M of tetrabutylammonium hexafluorophosphate ($TBAPF_6$, Sigma Aldrich, +99%) added as a supporting electrolyte. The working electrode was a Pt electrode from Radiometer-Tacussel exposing a geometrical area of 0.034 cm^2 and Pt wire was used as the counter electrode. All potentials are referenced against a saturated calomel electrode (SCE) recalibrated with Fc^+/Fc as standard ($E_{1/2}$ (Fc^+/Fc) = +0.380 V *vs* SCE in MeCN).[51] A conventional three-electrode cell (solution volume of 15 mL) was used and data were monitored on a PC-controlled potentiostat/galvanostat (Princeton Applied Research Inc. model 263A). Further mechanistic studies were performed using a three-electrode system with an Ag|AgCl|1M LiCl reference electrode and the potentiostat PGSTAT30 (Autolab, Metrohm Switzerland) with positive feedback iR compensation.

Molecular modeling.

All the structures were fully optimized within their respective spin state at the DH-SVPD level,[52] using as recommended by extensive benchmark test,[53,54] the PBE-QIDH double-hybrid density functional.[55] Scan energy reaction paths were evaluated using the PBE0 global-

hybrid density functional[56,57] corrected for dispersion with the D3(BJ) scheme[58] to alleviate the computational demand without deteriorating the accuracy. The first 20 vertical excitations of each compound were computed making use of the linear-response time-dependent density-functional theory (LR-TD-DFT) at the cc-pVTZ level,[59] taking advantage of the reliable description of the spectroscopic properties of chromophores[60] provided by PBE-QIDH. For both structure optimizations and vertical excitations, solvation was accounted for by using the (C)-PCM polarizable continuum model and setting the dielectric constant as the one of acetonitrile.[61] Structure optimizations were performed with the release C.01 of the Gaussian'16 program package[62] using tight convergence criteria and ultrafine integration grids. Vertical excitations were computed with the ORCA 4.2.1 release[63] using the RIJCOSX technique[64] with the automatic generation of appropriate auxiliary basis sets.[65] Band-shaped UV/vis absorption spectra were obtained by Gaussian function convolutions over the set vertical transitions using a full width at half maximum (FWHM) of 0.45 eV.

Acknowledgements

Financial support by the Grant Agency of the Czech Republic (21-13458S), and the Academy of Sciences of the Czech Republic (RVO: 61388955, 61388963), the Ministry of Education of the Czech Republic (Barrande Project 8J21FR016), the French Ministries of Europe and Foreign Affairs (MAE) and of Advanced Education, Research and Innovation (MESRI) (PHC Barrande, 2021 Project No. 46775VG), and the French National Research Agency, ANR ("E-StorIc" Project: ANR-14-CE05-0002), is gratefully acknowledged. E.B. acknowledges the GENCI CINES for HPC resources (Projects A0060810359 and A0080810359).

Conflict of interest

The authors declare no conflict of interest.

Keywords: electronic structure; electrostatic interactions; pyridinium; structure-activity relationships; supramolecular electrochemistry

Notes and References.

[1] J.-P. Launay, M. Verdaguer, in *Electrons in Molecules: From Basic Principles to Molecular Electronics*. Revised Edition (Ed. Oxford University Press), Oxford, **2018**.

[2] a) V. Balzani, L. Moggi, F. Scandola, in *Supramolecular Photochemistry* (Eds. V. Balzani, D. Reidel), Publishing Co.: Dordrecht, The Netherlands, **1987**; pp 1−28; b) V. Balzani, *Tetrahedron* **1992**, *48*, 10443−10514.

[3] P. L. Luisi, *Found. Chem*. **2002**, *4*, 183−200.

[4] a) J. Fortage, C. Peltier, F. Nastasi, F. Puntoriero, F. Tuyèras, S. Griveau, F. Bedioui, C. Adamo, I. Ciofini, S. Campagna, P. P. Lainé, *J. Am. Chem. Soc*. **2010**, *132*, 16700−16713; b) J. Fortage, C. Peltier, C. Perruchot, Y. Takemoto, Y. Teki, F. Bedioui, V. Marvaud, G. Dupeyre, L. Pospíšil, C. Adamo, M. Hromadová, I. Ciofini, P. P. Lainé, *J. Am. Chem. Soc*. **2012**, *134*, 2691−2705; c) Š. Lachmanová, G. Dupeyre, J. Tarábek, P. Ochsenbein, C. Perruchot, I. Ciofini, M. Hromadová, L. Pospíšil, P. P. Lainé, *J. Am. Chem. Soc*. **2015**, *137*, 11349−11364.

[5] J.-M. Lehn, *Angew. Chem. Int. Ed*. **2013**, *52*, 2836–2850; *Angew. Chem*. **2013**, *125*, 2906–2921.

[6] G. M. Whitesides, R. F. Ismagilov, *Science* **1999**, *284*, 89–92.

[7] J. H. van Esch, B. L. Feringa, *Angew. Chem. Int. Ed*. **2000**, *39*, 2263–2266; *Angew. Chem.* **2000**, *112*, 2351–2354.

[8] R. W. Saalfrank, H. Maid, A. Scheurer, *Angew. Chem. Int. Ed*. **2008**, *47*, 8794–8824; *Angew. Chem*. **2008**, *120*, 8924–8956.

[9] E. Ruijter, R. Scheffelaar, R. V. A. Orru, *Angew. Chem. Int. Ed*. **2011**, *50*, 6234–6246; *Angew. Chem*. **2011**, *123*, 6358–6371.

[10] D. H. Evans, *Chem. Rev*. **2008**, *108*, 2113−2144, and references therein.

[11] M. J. Weaver, X. Gao, *J. Phys. Chem.* **1993**, *97*, 332–338.

[12] Q. Xie, E. Pérez-Cordero, L. Echegoyen, *J. Am. Chem. Soc.* **1992**, *114*, 3978–3980.

[13] A. Gosset, L. Wilbraham, Š. Nováková Lachmanová, R. Sokolová, G. Dupeyre, F. Tuyèras, P. Ochsenbein, C. Perruchot, H.-P. Jacquot de Rouville, H. Randriamahazaka, L. Pospíšil, I. Ciofini, M. Hromadová, P. P. Lainé, *J. Am. Chem. Soc*. **2020**, *142*, 5162−5176.

[14] D. Gust, T. A. Moore, A. L. Moore, *Acc. Chem. Res*. **2001**, *34*, 40–48.

[15] M. R. Wasielewski, *J. Org. Chem*. **2006**, *71*, 5051–5066.

[16] C. Lambert, *Angew. Chem. Int. Ed.* **2005**, *44*, 7337–7339; *Angew. Chem*. **2005**, *117*, 7503–7505.

[17] D. M. Adams, L. Brus, C. E. D. Chidsey, S. Creager, C. Creutz, C. R. Kagan, P. V. Kamat, M. Lieberman, S. Lindsay, R. A. Marcus, R. M. Metzger, M. E. Michel-Beyerle,

J. R. Miller, M. D. Newton, D. R. Rolison, O. Sankey, K. S. Schanze, J. Yardley, X. Zhu, *J. Phys. Chem. B* **2003**, *107*, 6668–6697 and references therein.

[18] M. Mayor, J.-M. Lehn, *J. Am. Chem. Soc*. **1999**, *121*, 11231−11232.

[19] Here, prefix "super" has nothing to do with greater strength or intensity, but is related to the "supramolecular" nature of interactions according Balzani's acceptation (see Ref. [2]). It follows that functional assemblies that support these interactions are referred to as super-electrophores[13] (as super-molecules/supramolecular assemblies endowed of electrophoric properties).

[20] P. L. Boulas, M. Gòmez-Kaifer, L. Echegoyen, *Angew. Chem. Int. Ed*. **1998**, *37*, 216–247; *Angew. Chem*. **1998**, *110*, 226–258.

[21] D.-K. Seo, R. Hoffmann, *Theor. Chem. Acc*. **1999**, *102*, 23–32.

[22] a) A. Bondi, *J. Phys. Chem*. **1964**, *68*, 441−451; b) S. S. Batsanov, *Inorg. Mater*. **2001**, *37*, 871–885.

[23] L. Derdour, D. Skliar, *Chem. Eng. Sci.* **2014**, *106*, 275–292.

[24] T. Suzuki, Y. Kuroda, K. Wada, Y. Sakano, R. Katoono, *Chem. Lett*. **2014**, *43*, 887–889.

[25] a) N. G. Connelly, W. E. Geiger, *Chem. Rev*. **1996**, *96*, 877−910; b) J. Balej, *Electrochim. Acta* **1976**, *21*, 953−956.

[26] F. Teplý, M. Čížková, P. Slavíček, V. Kolivoška, J. Tarábek, M. Hromadová, L. Pospíšil, *J. Phys. Chem. C* **2012**, *116*, 3779−3786.

[27] D. Casarini, L. Lunazzi, A. Mazzanti, *Eur. J. Org. Chem*. **2010**, 2035–2056.

[28] T. Suzuki, T. Takeda, E. Ohta, K. Wada, R. Katoono, H. Kawai, K. Fujiwara, *Chem. Rec*. **2015**, *15*, 280–294 and references therein.

[29] T. Suzuki, J.-i. Nishida, T. Tsuji, *Angew. Chem., Int. Ed. Engl.* **1997**, *36*, 1329−1331; *Angew. Chem*. **1997**, *109*, 1387–1389.

[30] T. Suzuki, T. Takeda, H. Kawai, K. Fujiwara, *Pure Appl. Chem*. **2008**, *80*, 547−553.

[31] T. Suzuki, A. Migita, H. Higuchi, H. Kawai, K. Fujiwara, T. Tsuji, *Tetrahedron Lett*. **2003**, *44*, 6837–6840.

[32] Noteworthy, issues that underpin the research work by Suzuki et al. are disjointed from concerns and conclusions drawn out of the present work (see also Ref. [13] and associated Supporting Information).

[33] M. A. Oturan, P. Dostert, M. Strolin Benedetti, J. Moiroux, A. Anne, M. B. Fleury, *J. Electroanal. Chem*. **1988**, *242*, 171–179.

[34] K. Akiyama, S. Kubota, Y. Ikegami, *Chem. Lett*. **1981**, 469–472.

[35] J. I. Seeman, *Chem. Rev*. **1983**, *83*, 83–134.

[36] H. Li, B. Tirri, É. Brémond, J. C. Sancho-García, C. Adamo, *J. Org. Chem*. **2021**, *86*, 5538−5545.

[37] A. Dreuw, M. Head-Gordon, *J. Am. Chem. Soc*. **2004**, *126*, 4007–4016.

[38] Measurement of $|E_p–E_{p/2}|$, where $E_{p/2}$ is the half-peak potential, was found to be 39 mV, in line with a bi-electronic process for an irreversible system; see A. J. Bard, L. R. Faulkner, in *Electrochemical Methods. Fundamentals and Applications*, 2nd ed.; Wiley: New York, **2001**; Chapter 6.

[39] a) M. Goto, K. B. Oldham, *Anal. Chem*. **1973**, *45*, 2043–2050; b) J. C. Imbeaux, J.-M. Savéant, *J. Electroanal. Chem. Interfacial Electrochem.* **1973**, *44*, 169–187; c) F. Ammar, J.-M. Savéant, *J. Electroanal. Chem. Interfacial Electrochem.* **1973**, *47*, 215–221.

[40] M. Hromadová, L. Pospíšil, R. Sokolová, V. Kolivoška, *Collect. Czech. Chem. Commun*. **2011**, *76*, 1895–1908.

[41] L. Pospíšil, M. Hromadová, R. Sokolová, C. Lanza, *Electrochim. Acta* **2019**, *300*, 284–289.

[42] It is worth noting the lack of spin density at α sites, that explains absence of reactivity of $\mathbf{1}_{cis}^{-}$ as regards σ-dimerization.

[43] As shown in Table S6 (see Section S14 in the Supporting Information), dispersion effects are not the main driving force of the interactions leading to the stabilization of $\mathbf{1}_{cis}$ since structure optimization with or without dispersion correction leads to the $\mathbf{1}_{cis}$ pre-organized conformer.

[44] For species [*Z*] = 0, a caveat concerns DFT, which is not the fully adequate method to describe the system with large twist angles, *before the sudden transition*, where we normally end up with a biradical. While the latter species must be described by a multideterminant method, here we describe its electronic structure with a single determinant for consistency purposes. Errors typically introduced are underestimated energies for the large torsion angles. It remains nonetheless that the whole energy profile shows that the biradical species (including $\mathbf{1}_{2R}^{2-}$ in Figure 1A) does not exist. Most importantly, after the transition (at low θ angles), DFT accurately demonstrates that **2** is indeed the two-electron reduction product.

[45] Bruker, 2012, APEX II / APEX III / SAINT. Bruker AXS Inc., Madison, Wisconsin, USA.

[46] Bruker, 2001, SADABS. Bruker AXS Inc., Madison, Wisconsin, USA

[47] G. M. Sheldrick, *Acta Cryst*. *A* **2015**, *71*, 3–8.

[48] G. M. Sheldrick, *Acta Cryst. C* **2015**, *71*, 3–8.

[49] O. V. Dolomanov, L. J. Bourhis, R. J. Gildea, J. A. K. Howard, H. Puschmann, *J. Appl. Crystallogr*. **2009**, *42*, 339–341.

[50] K. Marat, SPINWORKS 4.25 Software, University of Manitoba. Available from: <http://www.umanitoba.ca/chemistry/nmr/spinworks>.

[51] V. V. Pavlishchuk, A. W. Addison, *Inorg. Chim. Acta* **2000**, *298*, 97–102.

[52] J. S. Garcia, É. Brémond, M. Campetella, I. Ciofini, C. Adamo, *J. Chem. Theory Comput.* **2019**, *15*, 2944–2953.

[53] É. Brémond, M. Savarese, N. Q. Su, A. J. Pérez-Jiménez, X. Xu, J. C. Sancho-Garcia, C. Adamo, *J. Chem. Theory Comput.* **2016**, *12*, 459–465.

[54] B. Tirri, I. Ciofini, J. C. Sancho-Garcia, C. Adamo, É. Brémond, *Int. J. Quantum Chem.* **2020**, *120*, e26233.

[55] É. Brémond, J. C. Sancho-Garcia, A. J. Pérez-Jiménez, C. Adamo, *J. Chem. Phys.* **2014**, *141*, 031101.

[56] C. Adamo, V. Barone, *J. Chem. Phys.* **1999**, *110*, 6158–6170.

[57] M. Ernzerhof, G. E. Scuseria, *J. Chem. Phys.* **1999**, *110*, 5029–5036.

[58] S. Grimme, S. Ehrlich, L. Goerigk, *J. Comput. Chem.* **2011**, *32*, 1456–1465.

[59] R. A. Kendall, T. H. Dunning Jr, R. J. Harrison, *J. Chem. Phys.* **1992**, *96*, 6796–6806.

[60] É. Brémond, I. Ciofini, J. C. Sancho-Garcia, C. Adamo, *Acc. Chem. Res.* **2016**, *49*, 1503–1513.

[61] J. Tomasi, B. Mennucci, R. Cammi, *Chem. Rev.* **2005**, *105*, 2999–3093.

[62] M. J. Frisch, G. W. Trucks, H. B. Schlegel, G. E. Scuseria, M. A. Robb, J. R. Cheeseman, G. Scalmani, V. Barone, G. A. Petersson, H. Nakatsuji, X. Li, M. Caricato, A. V. Marenich, J. Bloino, B. G. Janesko, R. Gomperts, B. Mennucci, H. P. Hratchian, J. V. Ortiz, A. F. Izmaylov, J. L. Sonnenberg, D. Williams-Young, F. Ding, F. Lipparini, F. Egidi, J. Goings, B. Peng, A. Petrone, T. Henderson, D. Ranasinghe, V. G. Zakrzewski, J. Gao, N. Rega, G. Zheng, W. Liang, M. Hada, M. Ehara, K. Toyota, R. Fukuda, J. Hasegawa, M. Ishida, T. Nakajima, Y. Honda, O. Kitao, H. Nakai, T. Vreven, K. Throssell, J. A. Montgomery Jr, J. E. Peralta, F. Ogliaro, M. J. Bearpark, J. J. Heyd, E. N. Brothers, K. N. Kudin, V. N. Staroverov, T. A. Keith, R. Kobayashi, J. Normand, K. Raghavachari, A. P. Rendell, J. C. Burant, S. S. Iyengar, J. Tomasi, M. Cossi, J. M. Millam, M. Klene, C. Adamo, R. Cammi, J. W. Ochterski, R. L. Martin, K. Morokuma,

O. Farkas, J. B. Foresman, D. J. Fox, *Gaussian 16*, Revision C.01; Gaussian, Inc., Wallingford CT, **2016**.

[63] F. Neese, Software update: the ORCA program system, version 4.0. Wiley Interdiscip. *Rev. Comput. Mol. Sci.* **2018**, *8*, e1327.

[64] F. Neese, F. Wennmohs, A. Hansen, U. Becker, *Chem. Phys.* **2009**, *356*, 98–109.

[65] G. L. Stoychev, A. A. Auer, F. Neese, *J. Chem. Theory Comput.* **2017**, *13*, 554–562.

Entry for the Table of Contents

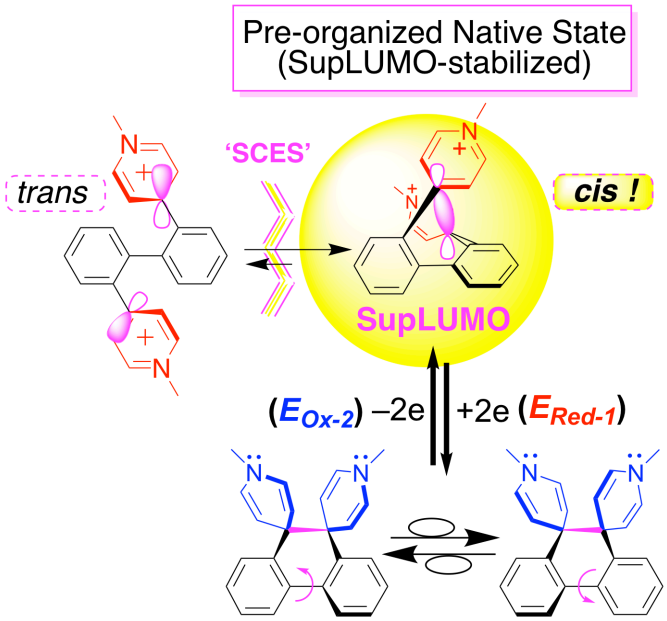

Upon sudden change of electronic structure (SCES), the doubly-electrophoric *trans* conformer of this redox-active assembly switches into a singly-superelectrophoric *cis* conformer on account of the synergistic interplay of electrophilic centers pertaining to the two pyridinium moieties. An extended LUMO (coined as supLUMO) indeed develops through space, which also plays the role of electron reservoir.